

Continuous Wave and Pulse EPR and ENDOR Study of Oxygenated Cobalt(II) Heme Model Systems

Sabine Van Doorslaer and Arthur Schweiger*

Physical Chemistry Laboratory, Swiss Federal Institute of Technology, 8092 Zurich, Switzerland

Received: October 14, 1999; In Final Form: January 10, 2000

Continuous wave (CW) and pulse electron paramagnetic resonance (EPR), and electron nuclear double resonance (ENDOR) techniques were used to study frozen solutions of (oxyCo)TPP(L) (TPP = tetraphenylporphyrin, L = pyridine, 1-methylimidazole). By using a combination of CW EPR at X-, Q-, and W-band and Davies-ENDOR at Q-band, the **g** and cobalt hyperfine matrices and their corresponding principal axes were, for the first time, determined in detail. The variation of the *g* values as a function of temperature was followed by Q-band CW EPR. The existing ambiguity about the assignment of one of the **g** principal axes to the O–O bond direction was analyzed in detail. By studying the different proton interactions with Mims-ENDOR at X-band, a considerable solvent effect was found. With hyperfine sublevel correlation (HYSCORE) at X-band and two-pulse ESEEM (electron spin-echo envelope modulation) at S-band, the hyperfine and nuclear quadrupole interactions of the nitrogen nuclei of the axial ligand and the TPP ligand were determined. All the magnetic parameters were analyzed as a function of the geometrical and electronic structure of the complexes.

1. Introduction

For several decades, the dioxygen storage and transport function of the iron-containing heme proteins, hemoglobin (Hb) and myoglobin (Mb), has been the subject of many spectroscopic studies. However, the analysis of the electronic and geometric structure is very difficult because of the fast autoxidation rates of these proteins and the fact that they are diamagnetic and therefore EPR-silent (EPR = electron paramagnetic resonance).

It has been found that many of the planar Co(II) complexes can reversibly form 1:1 adducts with molecular oxygen (for reviews see refs 1 and 2). These adducts are further related to the oxygen-carrying heme proteins since they possess a coordinated nitrogen base in the sixth coordination site of the metal ion. Both the oxygenated and the deoxygenated Co(II) adducts are paramagnetic and can thus be studied by EPR. Because of their unique features, these adducts have become of special interest as models for natural heme systems.^{1,2} In particular, cobalt(II) porphyrins are used as model systems because of their structural analogy with the porphyrin fragment of Hb and Mb, and the fact that the autoxidation is generally slower than in the case of the native proteins. The chemical substitution of ferrous protoporphyrin IX by cobaltous porphyrin in Hb and Mb³ opened the way for studying both the oxy and deoxy species of the proteins with EPR and electron nuclear double resonance (ENDOR) spectroscopy.^{4–9}

Although a number of EPR and ENDOR studies have been carried out on oxygenated synthetic cobalt systems,^{1,2} many problems are still left unsolved. The most pronounced ambiguity is the one concerning the assignment of the **g** principal axes to the dioxygen bond direction. Some of the authors^{1,10,11} ascribed the principal axis with the largest *g* value to the O–O bond direction in accordance with EPR studies on O₂[−] defects in alkali halide single crystals.¹² In oxycobalt myoglobin (oxyCoMb) single crystals Dickinson and Chien^{6,7} found at 77 K two oxy species and also assigned the largest *g* principal value to the

O–O bond directions. Hori et al.^{8,9} repeated these measurements at room temperature (RT) and 77 K. A comparison of the RT EPR and X-ray data of oxyCoMb revealed that the principal axis associated with the *g* value closest to the free electron value *g*_e is approximately oriented along the O–O bond. In a later work,⁹ they made the same assignment for the 77 K data. Subsequently, several authors assigned for different oxygenated Co(II) complexes the smallest *g* value^{13–16} or the middle *g* value to the O–O bond direction.¹⁷ This ambiguity has severe consequences for the interpretation of all the other magnetic parameters.

Moreover, in all studies done on frozen solutions of oxygenated cobalt(II) porphyrin systems, the **g** and **A**^{Co} matrices could not be determined accurately and simulations of the continuous wave EPR (CW EPR) spectra are found to be hardly convincing. This is due to the fact that the two matrices are orthorhombic and non-coaxial. The frozen solution CW EPR spectra recorded at X-band show strongly overlapping features, which complicate the evaluation of the parameters.

In this work, we report on a CW and pulse EPR and ENDOR study of frozen toluene solutions of oxygenated cobalt tetraphenylporphyrin(pyridine), (oxyCo)TPP(py) (**1a**), and oxygenated cobalt tetraphenylporphyrin(1-methylimidazole), (oxyCo)TPP-(1-MeIm) (**1b**). The two complexes have previously been investigated by means of CW EPR¹⁸ and three-pulse electron spin-echo envelope modulation (ESEEM) spectroscopy.^{17,19} In these studies, the ambiguity in the assignment of the **g** principal axes is not resolved and the reported data for **g** and **A**^{Co} are not convincing.

By means of CW EPR at X-, Q-, and W-band frequencies in combination with Davies-ENDOR at Q-band, the **g** and cobalt hyperfine matrices at low temperature are determined and the temperature dependence of the **g** principal values is investigated. The assignment of the **g** principal axes is discussed in detail.

The hyperfine interactions of the surrounding protons are determined by means of Mims-ENDOR at X-band. A pronounced solvent effect is observed. Finally, the hyperfine and nuclear quadrupole interactions of the pyridine (or 1-methylimidazole) binding nitrogen and of the porphyrin nitrogens are evaluated by means of two-dimensional HYSCORE at X-band in combination with two-pulse ESEEM at S-band. The HYSCORE technique is found to give more information than three-pulse ESEEM experiments.^{17,19} The observed interactions are interpreted in terms of internuclear distances and spin density distributions and are compared with values from the literature and from our recent study on CoTPP(py).²⁰

2. Materials and Methods

2.1. Sample Preparation. (Tetraphenylporphyrinato)cobaltate(II), CoTPP, from Aldrich was used without further purification. Pyridine and 1-methylimidazole were purchased from Fluka (pro analysis). As a solvent, toluene (Fluka, puriss., absolute, over molecular sieves) was used. Deuterated toluene-*d*₈ (>99.6% purity) was obtained from Cambridge Isotope Laboratories (CIL). Deuterated pyridine (py-*d*₅) (> 99% purity) was purchased from CIBA, and ¹⁵N-labeled pyridine ([¹⁵N]py) (>98% purity) was obtained from CIL. The porphyrin complex was dissolved in toluene containing 10 mM of pyridine or 1-methylimidazole. The final concentration of the CoTPP(py) and CoTPP(1-MeIm) complex was taken as 1 mM. After the components were mixed, the solution was transferred to an EPR tube and left open to air to obtain the oxygenated complexes.

¹⁵N-labeled (>99% purity) cobaltic tetraphenylporphyrin chloride, Co^{III}([¹⁵N]TPP)Cl was obtained from Porphyrin Products, Inc. To reduce Co^{III}([¹⁵N]TPP)Cl to the cobaltous state, it was dissolved in degassed CH₂Cl₂ in a concentration of 14 mM and then mixed with an equal volume of a solution of Na₂S₂O₄ in degassed H₂O (57 mM) for about 1 h. The CH₂Cl₂ phase was separated from the aqueous phase and vacuum-distilled. The remaining Co^{II}[¹⁵N]TPP was then treated in the same way as described above.

2.2. Equipment. The X-band CW EPR spectra were recorded at 80 K on a Bruker ESP 300 spectrometer (microwave (mw) frequency, 9.48 GHz), equipped with a liquid nitrogen cryostat. An mw power of 160 mW, a modulation amplitude of 0.05 mT, and a modulation frequency of 100 kHz were used. The X-band pulse EPR and ENDOR spectra (15 K throughout) were recorded on a Bruker ESP380 spectrometer (mw frequency, 9.71 GHz) equipped with a liquid Helium cryostat from Oxford Inc. The magnetic field was measured with a Bruker ER 035M NMR gaussmeter. In all pulse EPR and ENDOR measurements a repetition rate of 1 kHz was used. The observer positions were carefully chosen to scan through all the molecular orientations that contribute to the CW EPR spectrum.²¹

Mims-ENDOR.²² The spectra were recorded with the mw pulse sequence $\pi/2-\tau-\pi/2-T-\pi/2-\tau$ -echo, with pulse lengths of 16 ns. Time τ was varied from 96 to 600 ns in steps of 8 ns. A selective radio frequency (rf) π pulse of variable frequency ν_{rf} and length 10 μs was applied during the time interval T . The rf increment was set to 50 kHz.

HYSCORE (Hyperfine Sublevel Correlation).²³ The experiments were carried out with the pulse sequence $\pi/2-\tau-\pi/2-t_1-\pi-t_2-\pi/2-\tau$ -echo with pulse lengths $t_{\pi/2} = 24$ ns and $t_{\tau} = 16$ ns. The time intervals t_1 and t_2 were varied from 96 to 8272 ns in steps of 16 ns. Three τ values (96, 176, and 344 ns) were used to remove the blind spots. An eight-step phase cycle was used to eliminate unwanted echo contributions.

Matched HYSCORE.²⁴ The second and third $\pi/2$ pulse were replaced by matched pulses of length 88 ns. All other parameters were the same as those for unmatched HYSCORE.

The Q-band CW EPR and pulse ENDOR spectra were recorded on a home-built spectrometer (mw frequency, 35.39 GHz) equipped with a liquid Helium cryostat from Oxford Inc. and a Bruker ENDOR ER 5106 QTE probehead. The CW EPR spectra were recorded with a modulation amplitude of 0.2 mT and an mw power of 10 mW. All pulse ENDOR measurements were conducted at a repetition rate of 300 Hz and a temperature of 15 K.

Davies-ENDOR.²⁵ The spectra were measured with the sequence $\pi-T-\pi/2-\tau-\pi-\tau$ -echo, with mw pulse lengths of $t_{\pi/2} = 100$ ns and $t_{\tau} = 200$ ns and time intervals $\tau = 240$ ns and $T = 17 \mu\text{s}$. An rf π pulse of variable frequency ν_{rf} and length 15 μs was applied during time T .

The W-band CW EPR spectra were measured on a Bruker ELEXSYS 680 spectrometer (mw frequency, 94 GHz) equipped with cooling systems from Oxford Inc. and Cryogenics and a critically coupled Bruker TetraFlex probehead. An mw power of 1.78 mW, a modulation amplitude of 0.5 mT, and a modulation frequency of 100 kHz were used.

The S-band pulse EPR spectra were recorded on a home-built spectrometer (mw frequency, 3.78 GHz).

Two-Pulse ESEEM. The spectra were measured with the sequence $\pi/2-\tau-\pi-\tau$ -echo, with pulse lengths of 20 and 40 ns. Time τ was varied from 260 to 6240 ns in steps of 20 ns.

2.3. Theory. Oxygenated Co(II) complexes contain one unpaired electron which is mainly centered on the oxygen moiety. The spin Hamiltonian in frequency units can be written as

$$\mathcal{H} = \frac{\beta_e}{h} \mathbf{B}_0 \mathbf{g} \mathbf{S} + \mathbf{S} \mathbf{A}^{\text{Co}} \mathbf{I} + \mathcal{H}_{\text{nuc}} \quad (1)$$

The CW EPR spectra are dominated by the electron Zeeman interaction (first term) and the hyperfine interaction between the unpaired electron and the nuclear spin ($I = 7/2$) of cobalt (second term). \mathcal{H}_{nuc} describes the interactions with the surrounding nitrogen nuclei and the protons, which can be observed with ESEEM and ENDOR.

The hyperfine interactions of the cobalt nucleus and the protons are best determined with pulse ENDOR.²⁶ HYSCORE,²³ a two-dimensional experiment in which a mixing π pulse creates correlations between the nuclear coherences in two different electron spin (m_S) manifolds, is found to be the most appropriate method to study the magnetic parameters of the ligand nitrogens.

For an $S = 1/2$, $I = 1/2$ system (e.g. ¹⁵N), the nuclear transition frequencies in the two m_S manifolds are given by

$$\nu_{\alpha(\beta)} = \left[\left(\frac{A}{2} \pm \nu_I \right)^2 + \left(\frac{B}{2} \right)^2 \right]^{1/2} \quad (2)$$

with the nuclear Zeeman frequency $\nu_I = -g_n \beta_n B_0 / h$. A and B describe the secular and pseudosecular part of the hyperfine coupling. In the HYSCORE experiment, the correlations between the nuclear transitions lead to cross-peaks (ν_{α} , ν_{β}) and (ν_{β} , ν_{α}) in the 2D plots. The interpretation of HYSCORE spectra of disordered $S = 1/2$, $I = 1/2$ systems has been discussed by several authors.^{27,28}

The spin Hamiltonian of an $S = 1/2$, $I = 1$ system (e.g. ¹⁴N) can be described in terms of the \mathbf{g} matrix, the hyperfine matrix \mathbf{A} , and the nuclear quadrupole tensor \mathbf{Q} . The principal values Q_x , Q_y , and Q_z of the traceless \mathbf{Q} tensor are usually expressed by the quadrupole coupling constant $K = e^2 q Q / 4h$

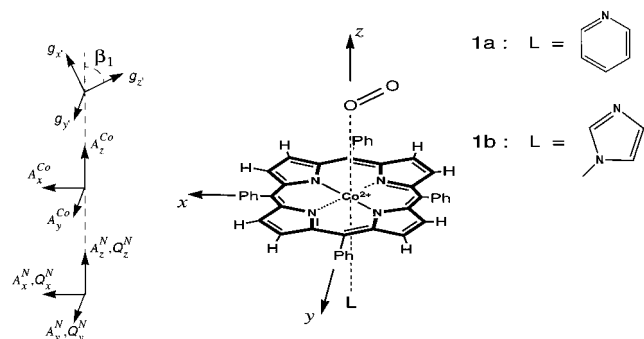


Figure 1. Structure of (oxyCo)TPP(py) (**1a**) and (oxyCo)TPP(1-MeIm) (**1b**) and orientation of the \mathbf{g} , \mathbf{A}^{Co} principal axes and the principal axes of \mathbf{A}^{N} and \mathbf{Q}^{N} of the sixth ligand with respect to the molecular frame (x , y , z).

and the asymmetry parameter η , with $Q_x = -K(1 - \eta)$, $Q_y = -K(1 + \eta)$, and $Q_z = 2K$. In the case of exact cancellation ($|A| \approx 2|v_l|$), the effective field experienced by the nucleus in one of the two m_S manifolds vanishes. The ESEEM frequencies within this manifold are therefore close to the nuclear quadrupole resonance (NQR) frequencies²⁹

$$\nu_0 = 2K\eta, \quad \nu_- = K(3 - \eta), \quad \nu_+ = K(3 + \eta) \quad (3)$$

HYSCORE spectra of disordered $S = 1/2$, $I = 1$ systems have been discussed by Dikanov et al.³⁰ The spectra are dominated by the cross-peaks between the double-quantum (DQ) frequencies³¹

$$\nu_{DQ}^{\alpha,\beta} = 2 \left[\left(\frac{a}{2} \pm v_l \right)^2 + K^2(3 + \eta^2) \right]^{1/2} \quad (4)$$

where a is the hyperfine coupling at a particular observer position.

2.4. Data Manipulation and Simulations. The data were processed with the program MATLAB 5.1 (The MathWorks, Inc., Natick, MA). The time traces of the HYSCORE spectra were baseline corrected with a third-order polynomial, apodized with a Hamming window, and zero filled. After 2D Fourier transformation, the absolute-value spectra were calculated. Both the Mims-ENDOR and HYSCORE spectra were recorded at different τ values and added together to eliminate τ dependent blind spots. The two-pulse ESEEM time traces were baseline corrected with an exponential function, apodized with a Hamming window, and zero filled. After 1D Fourier transformation, the absolute-value spectra were calculated. To get rid of dead time dependent line distortions in the absolute-value spectra, a cross-term averaging procedure³² was used.

The CW EPR, Davies-ENDOR, and two-pulse ESEEM spectra were simulated using MAGRES.³³ Simulations of the HYSCORE spectra were done with the program TRYSORE.³⁴ To obtain good starting values for the simulations of the HYSCORE spectra of $I = 1/2$ systems, the methods of Pöppel and Kevan²⁷ and Dikanov and Bowman²⁸ were used.

3. Results

3.1. \mathbf{g} and \mathbf{A}^{Co} Matrices. The X-band CW EPR spectrum of a frozen solution of (oxyCo)TPP(py) at 80 K is shown in Figure 2a. From this spectrum, the principal values of the \mathbf{g} and \mathbf{A}^{Co} matrices and their relative orientation are difficult to determine. To facilitate the analysis, also the Q-band (Figure 2b) and W-band (Figure 2c) CW EPR spectra were measured. Due to the large g strain and second-order effects in the hyperfine matrix, the cobalt hyperfine splittings are no longer resolved in

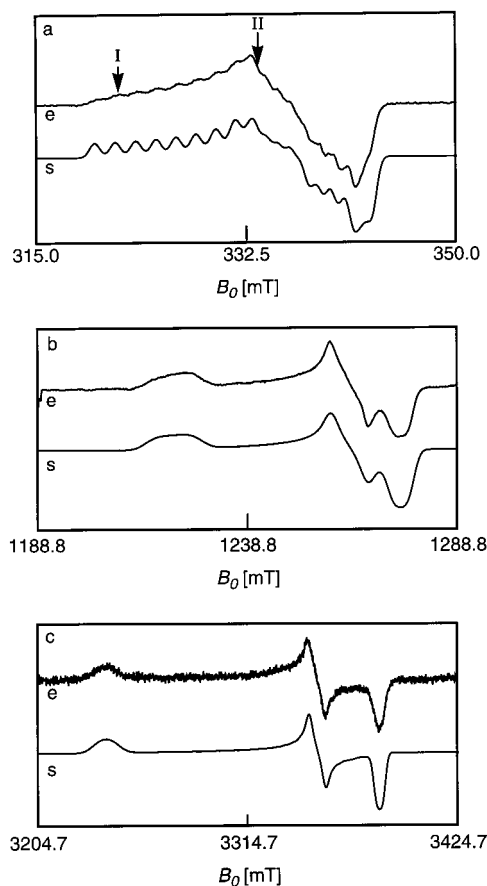


Figure 2. CW EPR spectra of (oxyCo)TPP(py) taken at 80 K. (e, experimental spectra; s, simulations): (a) X-band; (b) Q-band; (c) W-band.

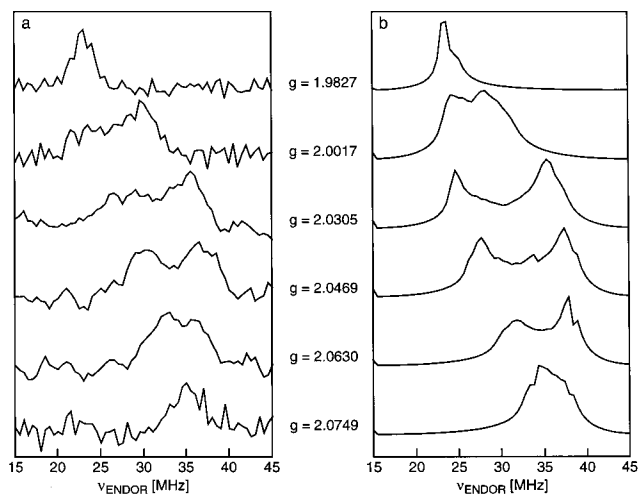


Figure 3. Q-band Davies-ENDOR spectra of (oxyCo)TPP(1-MeIm) taken at different observer positions: (a) experimental spectra; (b) simulations.

these spectra. The spectral features corresponding to the three principal g values overlap in the X-band spectrum but are nicely separated in the W-band EPR spectrum.

To determine the principal values of the \mathbf{A}^{Co} matrix and the relative orientation of the principal axes with respect to the \mathbf{g} principal axes, cobalt Davies-ENDOR spectra at Q-band were measured at different observer positions. Figure 3a shows some of the recorded spectra for (oxyCo)TPP(1-MeIm). The signals are weak and the cobalt nuclear quadrupole interaction is not

TABLE 1: Principal Values of the g and A^{Co} Matrices for (oxyCo)TPP(py) (1a) and (oxyCo)TPP(1-MeIm) (1b), Derived from CW EPR Spectra at X-, Q-, and W-Band Frequencies and from Q-Band Davies-ENDOR Spectra^a

	1a	1b	1a	1b
$g_x (\pm 0.0005)$	2.0020	2.0029	$A_y^{Co} (\pm 1.0 \text{ MHz})$	-21.4 -21.5
$g_y (\pm 0.0005)$	1.9827	1.9836	$A_z^{Co} (\pm 1.0 \text{ MHz})$	-22.7 -22.5
$g_z (\pm 0.0010)$	2.0705	2.0729	$\beta_1 (\pm 5^\circ)$	64 65
$A_x^{Co} (\pm 1.0 \text{ MHz})$	-53.0	-52.5		

^a The Euler angles for the g principal axes are $\alpha_1 = 0 \pm 5^\circ$ and $\gamma_1 = 0 \pm 5^\circ$; β_1 is given in the table. The Euler angles for the A^{Co} principal axes are $\alpha_2 = \beta_2 = \gamma_2 = 0 \pm 5^\circ$ (see Figure 1).

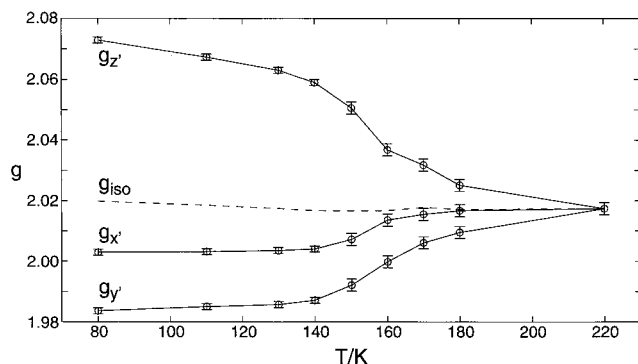


Figure 4. Variation of the g values of (oxyCo)TPP(1-MeIm) as a function of temperature, measured with Q-band CW EPR.

resolved. From the ENDOR line width, a maximum nuclear quadrupole coupling of 130 kHz is estimated.

The g and A^{Co} principal values and the Euler angles with respect to the molecular frame defined in Figure 1 are given in Table 1. The signs of the cobalt hyperfine values will be discussed later. The corresponding simulated EPR and ENDOR spectra are shown in Figures 2 and 3b. For the ENDOR simulations a line width of 1.8 MHz was assumed, which accounts for the unresolved nuclear quadrupole interactions. Although the values presented in Table 1 are the ones that produced the best simulations, it can be seen from Figure 3 that the ENDOR simulations are still not perfect. This is due to the fact that the nuclear quadrupole interaction is not taken into account directly. Although this interaction is small, it will have an influence both on the intensity and the position of the cobalt ENDOR lines. These effects cannot be simulated by means of a broader ENDOR line width. Surprisingly, for both complexes the cobalt hyperfine interactions are found to be equal within the experimental error.

It has been reported that upon cooling from 220 K to approximately 80 K, the CW EPR spectrum of oxygenated cobalt porphyrin complexes dissolved in toluene changes drastically.¹⁷ This is traced back to a reduced mobility of the O₂ moiety and of the whole complex at lower temperature. To check this behavior for the complexes under study, the temperature dependence of the g values has been studied. The change of the g values as a function of temperature can best be determined using W-band CW EPR. Since this requires a large amount of liquid helium (supercon sweep), the temperature dependence of the Q-band CW EPR spectra has been measured. Figure 4 shows for (oxyCo)TPP(1-MeIm) the change of the three g principal values and of the calculated isotropic value $g_{iso} = (g_x + g_y + g_z)/3$ as a function of temperature. The same trend was found for (oxyCo)TPP(py).

3.2. Interaction with the Surrounding Protons. Proton interactions can be measured with the Davies- and the Mims-ENDOR scheme. Since, at X-band, the proton signals overlap

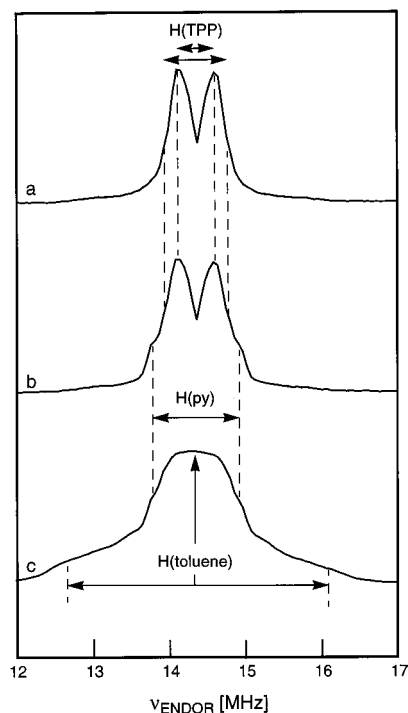


Figure 5. X-band Mims-ENDOR spectra at observer position I (see Figure 2a): (a) (oxyCo)TPP(py-*d*₅) in toluene-*d*₈; (b) (oxyCo)TPP(py) in toluene-*d*₈; (c) (oxyCo)TPP(py) in normal toluene.

with the cobalt ENDOR lines, only Mims-ENDOR, which has been found to be less sensitive to the strong cobalt couplings, has been used.

Figure 5a shows the X-band Mims-ENDOR spectrum of (oxyCo)TPP(py-*d*₅) in toluene-*d*₈ taken at observer position I (see Figure 2a). The observed couplings are due to the protons of the TPP ligand. A splitting of 0.4 MHz (± 0.1 MHz) is found for all observer positions in the EPR spectrum. For some observer positions, the peaks show weak shoulders with a maximal splitting of 0.7 ± 0.1 MHz (Figure 5a). Figure 5b shows the corresponding Mims-ENDOR spectrum of (oxyCo)TPP(py) in toluene-*d*₈. The additional splitting of 1.0 MHz observed in this spectrum can be ascribed to protons of the pyridine ligand. This splitting varies from 1.0 to 1.2 MHz when the observer position is changed. Figure 5c shows the Mims-ENDOR spectrum of (oxyCo)TPP(py) in normal toluene. A strong peak at the nuclear Zeeman frequency ν_H is observed, representing a large number of distant solvent protons. The broad peak with a maximal width of 3.4 MHz varies between 2.6 and 3.4 MHz as a function of the observer position.

The Mims-ENDOR spectra of (oxyCo)TPP(1-MeIm) in toluene-*d*₈ (not displayed) show splittings of 0.5 ± 0.1 MHz, which are assigned to the protons of TPP. In addition, weaker signals with a splitting of 1.3 ± 0.1 MHz are observed that can be assigned to the protons of 1-MeIm. The corresponding Mims-ENDOR spectra of the complex in toluene show besides a strong peak at ν_H , a broad peak with a width between 2.9 and 3.4 MHz symmetric to ν_H .

3.3. Interaction with the Surrounding Nitrogens. The interactions of the nitrogens have been investigated with ESEEM techniques. In particular, HYSCORE at different observer positions is well-suited for the determination of the magnetic parameters of nitrogen. Figure 6a shows the X-band HYSCORE spectrum of (oxyCo)TPP(py) at observer position II (see Figure 2a). To distinguish between the peaks of the pyridine and the porphyrin nitrogens, we also measured the corresponding

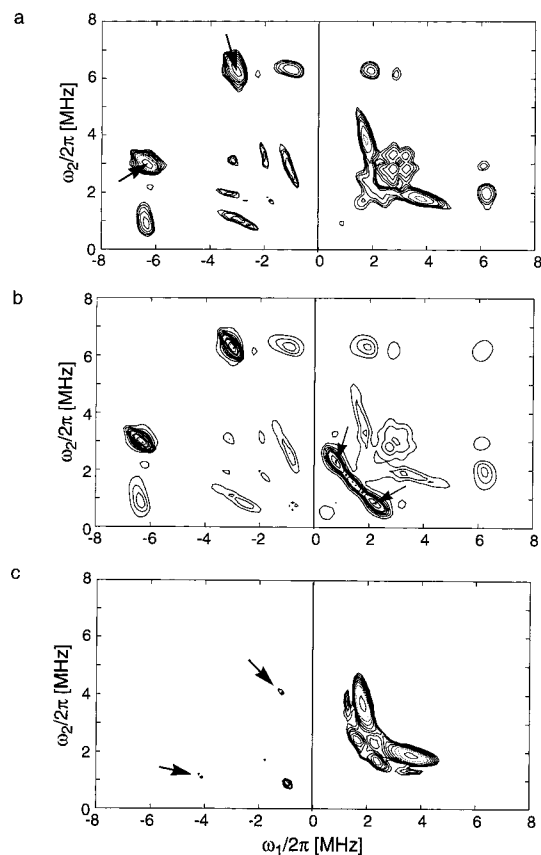


Figure 6. X-band nitrogen HYSCORE spectra at observer position II (see Figure 2a). (a) (oxyCo)TPP(py): The arrows indicate the DQ cross-peaks of the interaction with the ^{14}N of the pyridine ligand. (b) (oxyCo)- ^{15}N]TPP(py): The arrows indicate the peaks assigned to the ^{15}N nuclei of the porphyrin ligand. (c) (oxyCo)TPP(^{15}N]py): The arrows indicate the cross-peaks assigned to the ^{15}N nucleus of pyridine.

HYSCORE spectrum of (oxyCo) ^{15}N]TPP(py) (Figure 6b) and the matched HYSCORE spectrum of (oxyCo)TPP(^{15}N]py) (Figure 6c).

The weak signals of ^{15}N in (oxyCo)TPP(^{15}N]py) in the $(-, +)$ quadrant could only be observed with matched HYSCORE (arrows in Figure 6c). The corresponding ^{14}N signals of (oxyCo)TPP(py) are very strong (Figure 6a). The occurrence of the peaks in the $(-, +)$ quadrant indicates that $|A| > 2|\nu_{\text{N}}|$. The positions of DQ cross-peaks (arrows in Figure 6a) depend only slightly on the observer position, indicating that the hyperfine coupling is dominated by the isotropic part. Since for $I = 1/2$ spins nearly isotropic hyperfine couplings cause shallow modulations, the corresponding ^{15}N signals are hardly visible. In the case of ^{14}N , the deep modulations are caused by the nuclear quadrupole interaction.

Figure 7a shows the simulation of the ^{14}N HYSCORE spectrum of the pyridine nitrogen (observer position II), which should be compared with Figure 6b. The ^{15}N porphyrin interactions (arrows) are not considered in the simulation. The parameters are given in Table 2. Taking into account that the simulation was done with ideal pulses and that the TRYSORE program involves certain simplifications,³⁴ the agreement with the experiment is very good. The corresponding parameters for the ^{15}N nucleus were calculated by using the relation

$$|A_i^{15\text{N}}| = \left| \frac{g_{\text{N}}(^{14}\text{N})}{g_{\text{N}}(^{15}\text{N})} A_i^{14\text{N}} \right| \quad (5)$$

with $i = x, y, z$. The simulated ^{15}N cross-peaks (arrows in Figure

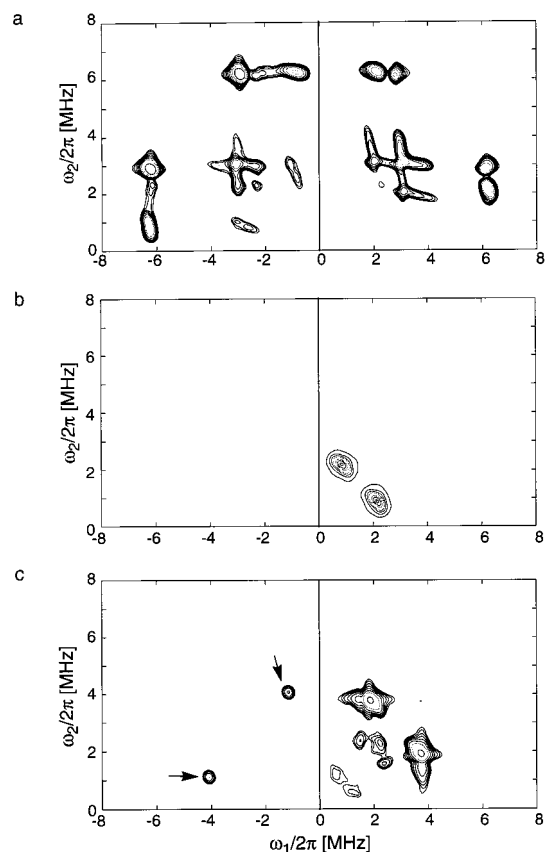


Figure 7. Simulated nitrogen HYSCORE spectra of (oxyCo)TPP(py) at observer position II: (a) ^{14}N nucleus of pyridine; (b) ^{15}N nuclei of the porphyrin ring; (c) ^{14}N nuclei of the porphyrin ring and ^{15}N nucleus of pyridine. The arrows indicate the cross-peaks assigned to the ^{15}N nucleus of pyridine.

TABLE 2: Principal Values of the Hyperfine Matrix and Nuclear Quadrupole Interactions of the Nitrogen of the Base of (oxyCo)TPP(py) (1a) and (oxyCo)TPP(1-MeIm) (1b), Derived from X-band HYSCORE and S-Band Two-Pulse ESEEM Spectra^a

	1a	1b
$A_x^{\text{N}} (\pm 0.1 \text{ MHz})$	3.4	3.2
$A_y^{\text{N}} (\pm 0.1 \text{ MHz})$	3.4	3.2
$A_z^{\text{N}} (\pm 0.1 \text{ MHz})$	3.7	3.8
$ e^2qQ/h (\pm 0.05 \text{ MHz})$	2.95	2.25
$\eta (\pm 0.02)$	0.23	0.10

^a The Euler angles for both A^{N} and Q^{N} are $\alpha_3 = \beta_3 = \gamma_3 = 0 \pm 5^\circ$ (see Figure 1).

7c) are in good agreement with the experiment (arrows in Figure 6c). For (oxyCo)TPP(1-MeIm), the same procedure was used (parameters see Table 2).

The ^{15}N peaks of the porphyrin are observed in the $(+, +)$ quadrant (arrows in Figure 6b). This implies that the coupling with these nitrogens is weak (i.e. $|A| < 2|\nu_{\text{N}}|$). The hyperfine interaction consists of a considerable anisotropic part, which causes the strong intensity of the ^{15}N peaks. At S-band, the hyperfine coupling will approximately be in exact cancellation ($|A| \approx 2|\nu_{\text{N}}|$), which allows for a straightforward determination of the nuclear quadrupole interaction (see theory). The combination of S-band and X-band HYSCORE spectra of (oxyCo)TPP(^{15}N]py) would represent an ideal data set for the determination of the nitrogen parameters. However in our experiment, the mixing π pulse at S-band was found to be too weak to correlate the nuclear coherences of the two m_S manifolds. We therefore used two-pulse ESEEM at S-band to measure the sharp features

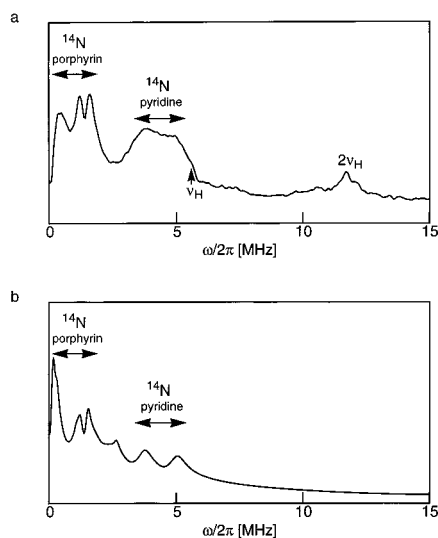


Figure 8. S-band two-pulse ESEEM spectrum of (oxyCo)TPP(py) (**1a**) and (oxyCo)TPP(1-MeIm) (**1b**), derived from CW EPR spectra at X-, Q-, and W-band frequencies and from Q-band Davies-ENDOR spectra.

that correspond to the NQR frequencies ν_0 , ν_- , and ν_+ (Figure 8a). The peaks around 4–5 MHz are due to the pyridine nitrogen and to protons.

It is difficult to get exact magnetic parameters for the pyrrole nitrogens, because the interactions are weak and the four nitrogens are not equivalent. Moreover, simulations show that for coinciding A^N and Q^N principal axes only the DQ cross-peaks are observed, in contradiction to the experiment. The computed hyperfine and nuclear quadrupole interactions are collected in Table 3. The four nitrogens are assumed to be geometrically equivalent with the A_z axes pointing approximately in the direction of the dioxygen fragment and the axes of the largest Q value pointing along the N–Co bond. The errors in the angles are rather large and an inequivalence of the four nitrogens cannot be ruled out.

Figure 7b shows the simulated ^{15}N pyrrole spectrum (compare with Figure 6b, arrows) and Figure 7c gives the corresponding spectrum of the ^{14}N pyrrole nitrogens (see Figure 6c). The simulation of the two-pulse ESEEM spectrum (Figure 8a) is shown in Figure 8b. The proton interactions are not considered, which explains the different shapes of the signal in the 4–5 MHz region. The observed NQR signals of the pyrrole nitrogens are nicely reproduced. For (oxyCo)TPP(1-MeIm), the same procedure was used (parameters, see Table 3).

4. Discussion

4.1. g and A^{Co} Matrices. For the assignment of the g principal axes with respect to the O–O bond direction, the work of Hori et al.^{8,9} on single crystals of (oxyCo)Mbs has to be discussed in more detail. For single crystals of (oxyprotoCo)-Mb and (oxymesocoCo)Mb the authors found one set of g values at room temperature (300 K) and two sets at 77 K. At room temperature, the observed g values for (oxymesocoCo)Mb are $g_1^{\text{RT}} = 2.065$, $g_2^{\text{RT}} = 2.009$, and $g_3^{\text{RT}} = 2.000$, with the g_3^{RT} principal axis (g value closest to g_e) close to the O–O bond direction as derived from X-ray data at 258 K. For the two forms at 77 K the g values $g_1^{\text{I}} = 2.072$, $g_2^{\text{I}} = 2.024$, $g_3^{\text{I}} = 1.975$ and $g_1^{\text{II}} = 2.080$, $g_2^{\text{II}} = 2.005$, $g_3^{\text{II}} = 1.987$ are reported with the g_1^{I} and g_1^{II} axes including an angle of approximately 90° . In agreement with the room-temperature data, the principal axes of the g values closest to g_e (g_2^{I} and g_2^{II}) are taken along the O–O bond direction in contrast with all previous assignments where the

dioxygen bond axis is assumed to be parallel to the principal axis of the largest g value.^{1,2}

Comparison of the (oxyCo)Mb data with B_{12r}O_2 in a single crystal of vitamin B_{12b} ¹¹ sheds a totally different light on the subject. For B_{12r}O_2 , one data set at high temperature (HT, 313 K) with $g_1^{\text{HT}} = 2.049$, $g_2^{\text{HT}} = 2.023$, and $g_3^{\text{HT}} = 2.009$, and one data set at low temperature (LT, 113 K) with $g_1^{\text{LT}} = 2.089$, $g_2^{\text{LT}} = 2.013$, and $g_3^{\text{LT}} = 1.993$ with different principal axes directions are observed. EPR measurements at various intermediate temperatures reveal a smooth change from g_i^{LT} to g_i^{HT} ($i = 1, 2, 3$). This change in g values is explained by an increasing thermal motion of the dioxygen fragment (wobbling around the low-temperature O–O bond direction combined with an oscillation). The similarities with (oxyCo)Mb are obvious. The finding that in (oxyCo)Mb the traces of the g^{RT} , g^{I} , and g^{II} matrices are approximately the same, and at room temperature only one data set is found, suggests a thermal motion of the O_2 fragment. Moreover, the fact that the g^{RT} principal axes directions are approximately between those of g^{I} and g^{II} , and the temperature dependence of the g values suggest a jumping between positions I and II with an additional wobbling at higher temperatures. The study on vitamin B_{12r}O_2 ¹¹ showed that the g values and the orientation of the principal axes changed rapidly in the temperature range 230–310 K. This implies that a comparison of the EPR data at 300 K and the X-ray data at 258 K may lead to wrong conclusions. Moreover, the assumption that the g value along the O–O bond direction should remain the same, whereas all other parameters should drastically change with increasing temperature, is very unlikely. The temperature dependence of the g matrix of vitamin B_{12r}O_2 ¹¹ shows that the smallest g^{HT} value smoothly changes to the smallest g^{LT} value. For (oxyCo)Mb, this would mean that the O–O bond direction taken at room temperature along g_3^{RT} coincides with the g_3^{I} (g_3^{II}) axis at 77 K. This is, however, not possible, since, from the ^{17}O hyperfine data of (oxyCo)Mb at 77 K,⁶ it is known that the g_3^{I} (g_3^{II}) axis is parallel to the lobe of the π^* orbital containing the unpaired electron. All these arguments are in favor of the assignment of the largest g value to the O–O bond direction, in accordance with earlier studies.^{1,2} Furthermore, Dickinson and Symons³⁵ reconsidered their data of (oxyCo)Mb and found that correspondence of the O–O direction with $g = 2.00$ presented them with severe difficulties. In their opinion, the only reasonable interpretation of their data and those of Hori^{8,9} could be obtained by taking g_{max} along the O–O bond. Finally, the angles β_1 for (oxyCo)TPP(py) and (oxyCo)TPP(1-MeIm) are in good agreement with X-ray studies on (oxyCo)Mb and cobalt porphyrins containing axially bound nitric oxide.^{36,37}

According to Figure 4, the g values of (oxyCo)TPP(py) and (oxyCo)TPP(1-MeIm) vary only slightly in the temperature range 80–140 K (the systematic error for the temperature range is about 10 K). From 140 to 180 K, a large change in the g values is observed, indicating an increased mobility of the O–O group and the whole molecule. Since the g matrix remains orthorhombic, the O–O fragment does not freely rotate around the Co–O bond. In a case of fast rotation of the O–O group around the Co–O bond, but slow motion of the molecule, the g matrix would be axial.¹⁷ Above 180 K, the O–O group and the molecule as a whole are rotating rapidly, giving rise to an isotropic EPR spectrum, in accordance with the melting point of toluene (178 K). The slight decrease of g_{iso} with increasing temperature can be explained by a weakening of the Co–O bond at higher temperatures. Finally, Figure 4 shows clearly that, in solution, upon increased mobility of the O–O group at higher

TABLE 3: Principal Values and Principal Axes Directions of the Hyperfine Matrix and Nuclear Quadrupole Tensor of the Four Nitrogens of the Porphyrin Ring of (oxyCo)TPP(py) (1a) and (oxyCo)TPP(1-MeIm) (1b), Obtained through Simulation from X-Band HSCORE Spectra and S-band Two-Pulse ESEEM Spectra

	$A_{x'}^N$ (± 0.2 MHz)	$A_{y'}^N$ (± 0.2 MHz)	$A_{z'}^N$ (± 0.2 MHz)	a_{iso}^N (± 0.2 MHz)	$ e^2qQ/h $ (± 0.1 MHz)	η (± 0.2)	α_4 ($\pm 20^\circ$)	α_5 ($\pm 20^\circ$)	β_4 ($\pm 20^\circ$)	β_5 ($\pm 20^\circ$)	γ_4 ($\pm 20^\circ$)	γ_5 ($\pm 20^\circ$)
1a	-1.3	-1.3	-0.4	-1.0	1.8	0.3	45	45	45	90	0	0
	-1.3	-1.3	-0.4	-1.0	1.8	0.3	135	135	45	90	0	0
	-1.3	-1.3	-0.4	-1.0	1.8	0.3	225	225	45	90	0	0
	-1.3	-1.3	-0.4	-1.0	1.8	0.3	315	315	45	90	0	0
1b	-1.2	-1.2	-0.3	-0.9	1.7	0.5	45	45	45	90	0	0
	-1.2	-1.2	-0.3	-0.9	1.7	0.5	135	135	45	90	0	0
	-1.2	-1.2	-0.3	-0.9	1.7	0.5	225	225	45	90	0	0
	-1.2	-1.2	-0.3	-0.9	1.7	0.5	315	315	45	90	0	0

temperature, the g values change, but their order stays the same. It is then very hard to imagine that in single crystals of (oxyCo)-Mb increased thermal motion of the dioxygen fragment would change the order of the three g values. This is again an argument in favor of the largest g value along the O–O bond.

For both complexes the cobalt hyperfine interactions are found to be equal within the experimental errors. The electronic structure of oxygenated Co(II) complexes is usually discussed in terms of the superoxide formulation ($\text{Co}^{\text{III}}\text{O}_2^-$)¹⁰ or by the spin-pairing model.^{1,38}

In the spin-pairing model, it is assumed that the two molecular orbitals (MO's) of the Co–O₂ fragment

$$\begin{aligned}\psi_1 &= \alpha' d_{z^2} + 4s\gamma + \beta\pi^*(x') + \alpha'' d_{xz} \\ \psi_2 &= \alpha'' d_{yz} + \epsilon\pi^*(y')\end{aligned}\quad (6)$$

affect the cobalt hyperfine interaction. The doubly occupied MO, ψ_1 , describes the overlap of a π^* (x') orbital of O₂ with the cobalt $3d_{z^2}$, $3d_{xz}$, and $4s$ orbitals. The second MO, ψ_2 , contains the unpaired electron. Since the two MO's are close in energy,³⁸ ψ_2 can polarize ψ_1 , resulting in a negative spin density in the $3d_{z^2}$, $3d_{xz}$, and $4s$ orbitals.

The principal values of the cobalt hyperfine matrix are then found to be

$$\begin{aligned}A_x &= -1/2 T_{||} + a_{iso}^{\text{Co}} + 2/7(f - 2l - h) \\ A_y &= -1/2 T_{||} + a_{iso}^{\text{Co}} + 2/7(f + l + 2h) \\ A_z &= + T_{||} + a_{iso}^{\text{Co}} + 2/7(-2f + l - h)\end{aligned}\quad (7)$$

where $T_{||} = 3$ MHz is the direct point dipole–dipole interaction between the unpaired electron in the $\pi^*(y')$ orbital and the cobalt nuclear spin³⁸ and $f = P\rho_0 U_{\text{Co-O}}(\alpha')^2$, $h = P\rho_0 U_{\text{Co-O}}(\alpha'')^2$, and $l = P(\alpha'')^2$ describe the indirect spin polarization of d_{z^2} and d_{xz} and the direct hyperfine contribution from d_{yz} , respectively. $U_{\text{Co-O}}$ is the spin-polarization constant, ρ_0 is the spin density on the adjacent oxygen, and $P = g_e\beta_e g_n\beta_n \langle r^{-3} \rangle_{3d} = 600$ MHz.³⁸

Hoffman et al.,¹⁰ on the other hand, proposed a mechanism for the description of the anisotropic cobalt hyperfine interaction in a MO (ψ_1) involving the antibonding $\pi^*(y')$ oxygen orbital and the cobalt $3d_{yz}$ orbital (π back-bonding). In eq 7, this implies that $f = h = 0$. This assumption leads to $(\alpha'')^2 \approx 0.05$ for both complexes, which essentially means that almost complete electron transfer from cobalt to oxygen has taken place (superoxo formulation). The model does, however, not fully describe the anisotropy of the cobalt hyperfine matrix.

The spin-pairing model does not allow for a large transfer of the unpaired electron to the oxygen. Equation 7 leads to $f + h = 6.8$ MHz and $l + h = 36.2$ MHz for both complexes under study. If f and h are taken positive (which is expected in a spin-

pairing model), an upper limit for $(\alpha'')^2$ of 0.06 is found. Since the individual values of f , h , and l may not be derived from eq 7, f or h can actually be negative implying direct interaction rather than spin polarization. In fact, for some oxygenated Co(II) complexes, $f + h$ was found to be negative.^{1,11} Thus, the spin-pairing model appears to be incomplete to describe the cobalt hyperfine structure. Moreover, the cobalt hyperfine interaction is virtually independent of the axial base. For base-free (oxyCo)TPP, however, significantly larger (absolute) values are found.¹

Upon addition of a nitrogen base to CoTPP, the unpaired electron resides in the $3d_{z^2}(\text{Co}) + p_\sigma(\text{N})$ orbital. The $3d_{yz}$ ($3d_{xz}$) orbital combine with the $p_\pi(\text{N})$ orbital, but the energy shift is smaller than the one for the $3d_{z^2}$ orbital. If spin polarization of the $3d_{z^2}$ orbital plays an important role for the oxygenated complexes, a change of the base strength would have a significant influence on the cobalt hyperfine interaction, which is not observed. The difference in the cobalt hyperfine interaction for (oxyCo)TPP and (oxyCo)TPP(B) (B = nitrogen base) seems mostly to be due to the change in the $3d_{yz}$ level, spin-polarization of the $3d_{z^2}$ orbital plays only a minor role for this interaction.

Two recent studies report on the \mathbf{g} and \mathbf{A}^{Co} matrices of (oxyCo)TPP(1MeIm) in toluene.^{16,17} The first study¹⁶ involves the investigation of (oxyCo)[(o-R)TPP](1MeIm) (where R = -H, -NHCOC(CH₃)₃, -NHCOC(CH₃), -NHCONHC₆H₅, an ortho substituent on one of the four meso phenyls of TPP) in different solvents. The \mathbf{g} and \mathbf{A}^{Co} matrices were assumed to be coaxial, which is shown to be incorrect. Accordingly, their results for (oxyCo)TPP(1MeIm) in toluene deviate considerably from ours. For the different systems, the authors calculated the $3d$ orbital spin density of cobalt from the \mathbf{A}^{Co} principal values. In view of the present study, these data should be revised. In the second work,¹⁷ the \mathbf{g} and \mathbf{A}^{Co} matrices were determined from X- and Q-band CW EPR spectra. Although the authors included the non-coaxiality of the \mathbf{g} and \mathbf{A}^{Co} principal axes, there is still a discrepancy with our results (overestimation of A_x^{Co} and underestimation of A_y^{Co} and A_z^{Co}). The larger experimental data set used in the present work (CW EPR at three microwave frequencies in combination with ENDOR) justifies our results. Moreover, the simulation shown in ref 17 do not match the experimental spectra.

4.2. Proton Interactions. For several ferrous porphyrin systems, the P_{50} value of oxygen binding was found to decrease with increasing polarity of the solvent.³⁹ The same effects have been observed for cobaltous porphyrins.² This demonstrates the role of the solvent polarity in governing dioxygen affinity. For both complexes under study, the largest proton hyperfine coupling can be assigned to toluene protons. This proves the interaction between the solvent molecules and the dioxygen moiety.

Assuming $a_{iso} = 0$, the coupling of 0.4–0.7 MHz for the TPP protons of both complexes corresponds to a distance of

0.5–0.6 nm. The protons of the porphyrin ring and the ortho-protons of the phenyl groups fall within this range. The dioxygen is clearly not stabilized by a hydrogen bound to the ortho-proton of one of the phenyl groups. When the ortho-protons are replaced by electron withdrawing amide groups (picket fence porphyrins), an amide proton on the picket fence is believed to interact with the dioxygen, explaining the increased oxygen affinity of these complexes.^{16,40–42}

For (oxyCo)TPP(py) a maximum splitting of 1.0–1.2 MHz is observed for the pyridine protons, a coupling which is probably due to the ortho-protons of pyridine. For CoTPP(py), a maximum splitting of 7.1 MHz was observed for these protons.²⁰ The decrease of the proton hyperfine coupling reflects the electron withdrawal by the dioxygen molecule, which is also manifested in the cobalt hyperfine coupling. For (oxyCo)TPP(1-MeIm), an analogous maximal splitting of 1.3 ± 0.1 MHz was found for the 1-MeIm protons.

4.3. Nitrogen Interactions. For (oxyCo)TPP(py), the observed ¹⁴N hyperfine interaction of the pyridine ligand consists of an isotropic part $a_{\text{iso}} = 3.5$ MHz and a dipolar part ($-0.1, -0.1, +0.2$) MHz. From a_{iso} , a spin density on the nitrogen of $\rho_{\text{N}} = 0.0023$ ($\rho_{\text{N}} = a_{\text{iso}}/a_0$ with $a_0 = 1538.22$ MHz⁴³) is obtained, which is about a factor of 10 smaller than is found for oxygen free CoTPP(py).²⁰ This again agrees with the withdrawal of the unpaired electron by the oxygen. From the dipolar part, a distance $r = 0.39 \pm 0.06$ nm between the nitrogen nucleus and the unpaired electron can be derived.⁴⁴

For the pyridine ¹⁴N nuclear quadrupole interaction, we evaluate the values $|e^2qQ/h| = 2.95$ MHz and $\eta = 0.23$. Hsieh et al.⁴⁶ found from nuclear quadrupole resonance experiments the values $|e^2qQ/h| = 4.584$ MHz and $\eta = 0.396$ for the free pyridine molecule. These authors also observed that upon coordination of pyridine with a Lewis acid, the electric field gradient at the nitrogen nucleus decreases. For CoTPP(py), $|e^2qQ/h|$ decreases to 3.4 MHz,²⁰ and upon oxygenation, this value decreases even further. Hsieh et al.⁴⁶ found a linear relation between $|h/e^2qQ|$ and η . Using their simplified equation, $\eta = 0.23$ corresponds with $|e^2qQ/h| = 3.05$ MHz, which agrees nicely with our findings.

For the interaction with the pyridine nitrogen in (oxyCo)TPP(py), Magliozzo et al.¹⁹ derived from three-pulse ESEEM the parameters $A_{\text{xx}} = 2.9$ MHz, $A_{\text{yy}} = 3.4$ MHz, $A_{\text{zz}} = 3.9$ MHz, $|e^2qQ/h| = 2.9$ MHz, $\eta = 0.2$, $\alpha = 60^\circ$, $\beta = \gamma = 0^\circ$, with the Euler angles α , β , and γ , describing the relations between the principal axes of \mathbf{A}^{N} and \mathbf{Q}^{N} . The orthorhombicity of the \mathbf{A}^{N} matrix and the noncoaxiality of the \mathbf{A}^{N} and \mathbf{Q}^{N} axes could not be confirmed by our measurements. However, the shallow ¹⁵N modulations do not allow for such a large anisotropy. The inconsistency with our results may originate from the fact that the authors measured the three-pulse ESEEM spectrum only at one observer position (approximately position I, Figure 2a) and for only one τ value (blind spots). Because of the small \mathbf{g} anisotropy, they averaged in the powder simulations over all possible magnetic field orientations. Our measurements show, however, a distinct orientation selectivity. The authors had to assume an orthorhombic hyperfine matrix to account for some of the spectral features, which in fact result from poor orientation selection. We could nicely simulate the HYSCORE spectra at different observer positions by using the parameter set given in Table 2.

Magliozzo et al.¹⁹ also had difficulties in figuring out whether the largest principal axis of the \mathbf{Q}^{N} tensor is aligned along the Co–N bond direction or along the $2p_z$ orbital of the pyridine nitrogen. Information about this direction can be derived from

the broad single-quantum peaks, which are usually lost in three-pulse ESEEM experiments due to the instrumental dead time. In the HYSCORE spectra, these peaks are clearly seen, so that the assignment of the axes can easily be done through simulation. The orientation of the \mathbf{Q}^{N} tensor suggests that the nuclear quadrupole coupling is mainly governed by the p_σ population and not by the population in the pyridine π system. In the latter case, the largest Q value (in absolute value) would be found perpendicular to the Co–N direction.

For (oxyCo)TPP(1-MeIm), the hyperfine data of the coordinating ¹⁴N of 1-MeIm are very close to those observed in (oxyCo)TPP(py) ($a_{\text{iso}} = 3.4$ MHz, $\rho_{\text{N}} = 0.0022$, and $r = 0.32 \pm 0.04$ nm), in agreement with the finding that the cobalt hyperfine interaction is similar in both complexes. The difference in the ¹⁴N \mathbf{Q}^{N} tensor is, however, significant. For free imidazole the NQR data $|e^2qQ/h| = 3.220$ MHz and $\eta = 0.119$ are reported.⁴⁵ For 1-MeIm, similar values are expected. Both $|e^2qQ/h|$ and η are smaller than the ones for the free pyridine,⁴⁶ as is also reflected in our data. Furthermore, the coordination of 1-MeIm to the Lewis acid (oxyCo)TPP reduces the value of $|e^2qQ/h|$ in accordance with the observations for (oxyCo)TPP(py). Using three-pulse ESEEM, Lee et al.¹⁶ found for the ¹⁴N interaction $a_{\text{iso}} = 3.54 \pm 0.06$ MHz, $r = 0.34 \pm 0.02$ nm, $|e^2qQ/h| = 2.39 \pm 0.07$ MHz, and $\eta = 0.88 \pm 0.13$. The difference from our results can again be ascribed to the shortcomings of the applied technique (1D experiment and only one π value). It should be noticed that the error limits given by Lee et al.¹⁶ were clearly underestimated.

Until now, the remote nitrogen of 1-MeIm has not been discussed. On the basis of the data we found for the binding nitrogen of 1-MeIm, we expect the hyperfine interaction with the remote nitrogen to be very small. For free imidazole the NQR data for the amino nitrogen $|e^2qQ/h| = 1.391$ MHz and $\eta = 0.930$ are reported.⁴⁵ Simulations of HYSCORE spectra using an isotropic hyperfine interaction of 100 kHz and the nuclear quadrupole data from the free imidazole showed two broad diagonal peaks at ≈ 1.2 and ≈ 2.3 MHz in the (+,+) quadrant. In the HYSCORE spectra of (oxyCo)TPP(1-MeIm), such peaks were indeed observed, confirming that the hyperfine interaction with the remote nitrogen is small. Slight changes in the nuclear quadrupole parameters had virtually no influence on the data.

The hyperfine interactions with the porphyrin nitrogens of (oxyCo)TPP(py) ((oxyCo)TPP(1-MeIm)), can be split into an isotropic part with $a_{\text{iso}} = -1$ (-0.9) MHz and a dipolar part with ($-0.3, -0.3, +0.6$) MHz. The dipolar part corresponds to a distance $r = 0.27 \pm 0.04$ nm between the nitrogen and the unpaired electron. The orientation of the hyperfine principal axes supports again the assumption that an almost complete transfer of the unpaired electron from cobalt to the dioxygen has taken place, as suggested by Hoffman et al.¹⁰ A comparison of the parameters of the pyrrole nitrogens of CoTPP(py) and (oxyCo)TPP(py) shows that the electron withdrawal by the oxygen has a strong influence on the hyperfine interaction. For CoTPP(py) the nitrogen orbital involved in the MO containing the unpaired electron is an sp^2 -type hybrid; hence, there is direct spin density in the nitrogen 2s orbital. This results in the positive a_{iso} value. For (oxyCo)TPP(py), we found a negative a_{iso} value of about -1 MHz for the pyrrole nitrogens, indicating that the s -spin density is mainly due to polarization effects. This is in agreement with the ENDOR data of N,N' -ethylenebis(acetylacetonatiminato)cobalt(II), Co(acacen).^{47,48} For Co(acacen) a $|^2A, yz\rangle$ ground state is assumed and negative a_{iso} values of about -3.5 MHz are reported for the binding nitrogen. This situation resembles

the case of (oxyCo)TPP(py), where the unpaired electron resides in a MO to which the $3d_{yz}$ orbital contributes (see eq 6).

In contrast to the hyperfine data, the nuclear quadrupole parameters of the pyrrole nitrogens change only slightly upon oxygenation of the CoTPP(py) complex (for CoTPP(py): $|e^2qQ/h| = 1.8$ MHz; $\eta = 0.55$ ²⁰). This is because the hyperfine interaction is determined by the distribution of the unpaired electron, whereas the nuclear quadrupole tensor is determined by the electric field gradient at the ¹⁴N nucleus generated by the surrounding charges. It is interesting to note that the nuclear quadrupole parameters of the binding nitrogens of Co(acacen) resemble those reported here for the pyrrole nitrogens (N1, $|e^2qQ/h| = 1.79$ MHz, $\eta = 0.69$; N2, $|e^2qQ/h| = 1.84$ MHz, $\eta = 0.59$ ⁴⁷). This may again be ascribed to the electronic similarities as described above.

5. Conclusion

Frozen toluene solutions of two oxygenated Co(II) heme model systems, (oxyCo)TPP(py) and (oxyCo)TPP(1-MeIm), are studied by means of different one- and two-dimensional EPR and ENDOR methods at microwave frequencies between 3.7 and 95 GHz. The use of these methods together with isotopic substitutions allows a detailed analysis of these systems.

(a) The **g** and **A**^{Co} matrices and the direction of the principal axes are determined by CW EPR at X-, Q-, and W-bands and Davies-ENDOR at Q-band. The change of the *g* values as a function of temperature is studied by means of Q-band CW EPR. The ambiguity in the assignment of the **g** principal axes to the dioxygen bond direction is discussed in detail. Strong arguments in favor of the assignment of *g*_{max} along the O–O bond are given. On the basis of the interpretation of the cobalt hyperfine data, we found that the compounds studied in this work are adequately described by the Co^{III}O₂⁻ model rather than the spin-pairing model.

(b) The proton couplings (intra- and extramolecular) are investigated using Mims-ENDOR at X-band. A considerable solvent effect is observed.

(c) By means of HYSCORE at X-band and two-pulse ESEEM at S-band, the hyperfine and nuclear quadrupole interactions of the nitrogen of the axial ligand and the nitrogens in the porphyrin ring are investigated. The hyperfine interaction with the axial ligand nitrogen is found to be predominantly isotropic. The nuclear quadrupole tensor points along the Co–N bond direction. The influence of the base is discussed in detail. For the pyrrole nitrogens, **A**^N and **Q**^N are not coaxial. The hyperfine interactions have a considerable anisotropic contribution arising from the dipolar interaction with the unpaired electron on the dioxygen fragment, and the isotropic hyperfine coupling is found to be negative. A change of the axial ligand has no significant influence on this interaction.

In this paper, the potential of EPR and ENDOR techniques at different microwave frequencies is clearly demonstrated.

Acknowledgment. This research has been supported by the Swiss National Science Foundation. Dr. Gunnar Jeschke and Prof. Dr. W. Spiess of the Max Plank Institut in Mainz, Germany, are gratefully thanked for the W-band measurements. Dr. Igor Gromov is kindly thanked for his helpful assistance with the Q-band spectrometer. We are grateful to Dr. R. Bachmann for helpful discussions.

References and Notes

- (1) Smith, T. D.; Pilbrow, J. R. *Coord. Chem. Rev.* **1981**, *39*, 295.

- (2) Jones, R. D.; Summerville, D. A.; Basolo, F. *Chem. Rev.* **1979**, *79*, 139.
- (3) Hoffman, B. M.; Petering, D. H. *Proc. Natl. Acad. Sci. U.S.A.* **1970**, *67*, 637.
- (4) Ikeda-Saito, M.; Brunori, M.; Yonetani, T. *Biochim. Biophys. Acta* **1978**, *533*, 173, and further references cited therein.
- (5) Hüttermann, J.; Stabler, R. In *Electron Magnetic Resonance of Disordered Systems*; Yordanov, N. D., Ed.; World Scientific: Singapore, 1989; pp 127–148, and further references cited therein.
- (6) Dickinson, L. C.; Chien, J. C. W. *Proc. Natl. Acad. Sci. U.S.A.* **1980**, *77*, 1235.
- (7) Chien, J. C. W.; Dickinson, L. C. *Proc. Natl. Acad. Sci. U.S.A.* **1972**, *69*, 2783.
- (8) Hori, H.; Ikeda-Saito, M.; Yonetani, T. *Nature* **1980**, *288*, 501.
- (9) Hori, H.; Ikeda-Saito, M.; Yonetani, T. *J. Biol. Chem.* **1982**, *257*, 3636.
- (10) Hoffman, B. M.; Diemente, D. L.; Basolo, F. *J. Am. Chem. Soc.* **1970**, *92*, 61.
- (11) Jörin, E.; Schweiger, A.; Günthard, Hs. H. *J. Am. Chem. Soc.* **1983**, *105*, 4277.
- (12) Zeller, H. R.; Känzig, W. *Helv. Phys. Acta* **1967**, *40*, 845.
- (13) Lee, H. C.; Peisach, J.; Dou, Y.; Ikeda-Saito, M. *Biochemistry* **1994**, *44*, 7609.
- (14) Lee, H. C.; Ikeda-Saito, M.; Yonetani, T.; Magiozzo, R. S.; Peisach, J. *Biochemistry* **1992**, *31*, 7274.
- (15) Lee, H. C.; Peisach, J.; Tsuneshige, A.; Yonetani, T. *Biochemistry* **1995**, *34*, 6883.
- (16) Lee, H. C.; Scheuring, E.; Peisach, J.; Chance, M. R. *J. Am. Chem. Soc.* **1997**, *119*, 12201.
- (17) Bowen, J. H.; Shokhirev, N. V.; Raitsimring, A. M.; Buttlare, D. H.; Walker, F. A. *J. Phys. Chem. B* **1997**, *101*, 8683.
- (18) Walker, F. A. *J. Am. Chem. Soc.* **1970**, *92*, 4235.
- (19) Magliozzo, R. S.; McCracken, J.; Peisach, J. *Biochemistry* **1987**, *26*, 7923.
- (20) Van Doorslaer, S.; Bachmann, R.; Schweiger, A. *J. Phys. Chem.* **1999**, *103*, 5446.
- (21) Rist, G.; Hyde, J. J. *J. Chem. Phys.* **1970**, *52*, 4633.
- (22) Mims, W. B. *Proc. R. Soc. London* **1965**, *283*, 452.
- (23) Höfer, P.; Grupp, A.; Nebenführ, H.; Mehring, M. *Chem. Phys. Lett.* **1986**, *132*, 279.
- (24) Jeschke, G.; Rakhmatullin, R.; Schweiger, A. *J. Magn. Reson.* **1998**, *131*, 261.
- (25) Davies, E. R. *Phys. Lett.* **1974**, *A47*, 1.
- (26) Gemperle, C.; Schweiger, A. *Chem. Rev.* **1991**, *91*, 1481.
- (27) Pöppel, A.; Kevan, L. *J. Phys. Chem.* **1996**, *100*, 3387.
- (28) Dikanov, S. A.; Bowman, M. K. *J. Magn. Reson.* **1995**, *A116*, 125.
- (29) Flanagan, H. L.; Singel, D. J. *J. Chem. Phys.* **1987**, *87*, 5606.
- (30) Dikanov, S. A.; Xun, L.; Karpel, A. B.; Tyryshkin, A. M.; Bowman, M. K. *J. Am. Chem. Soc.* **1996**, *118*, 8408.
- (31) Dikanov, S. A.; Tsvetkov, Yu. D.; Bowman, M. K.; Astashkin, A. V. *Chem. Phys. Lett.* **1982**, *90*, 149.
- (32) Van Doorslaer, S.; Sierra, G.; Schweiger, A. *J. Magn. Reson.* **1999**, *136*, 152.
- (33) Keijzers, C. P.; Reijerse, E. J.; Stam, P.; Dumont, M. F.; Gribnau, M. C. M. *J. Chem. Soc., Faraday Trans. 1* **1987**, *83*, 3493.
- (34) Szosenfogel, R.; Goldfarb, D. *Mol. Phys.* **1998**, *95*, 1295.
- (35) Dickinson, L. C.; Symons, M. C. R. *Chem. Soc. Rev.* **1993**, *12*, 387.
- (36) Brucker, E. A.; Olson, J. S.; Phillips, G. N.; Dou, Y.; Ikeda-Saito, M. *J. Biol. Chem.* **1996**, *271*, 25419.
- (37) Richter-Addo, G. B.; Hodge, S. J.; Yi, G.-B.; Khan, M. A.; Ma, T.; Van Caemelbecke, E.; Guo, N.; Kadish, K. M. *Inorg. Chem.* **1996**, *35*, 6530.
- (38) Trovog, B. S.; Kitko, D. J.; Drago, R. S. *J. Am. Chem. Soc.* **1976**, *98*, 5144.
- (39) Momenteau, M.; Reed, C. A. *Chem. Rev.* **1994**, *94*, 659.
- (40) Mispelter, J.; Momenteau, M.; Lavalette, D.; Lhoste, J.-M. *J. Am. Chem. Soc.* **1983**, *105*, 5165.
- (41) Gerathanassis, I. P.; Momenteau, M.; Looock, B. *J. Am. Chem. Soc.* **1989**, *111*, 7006.
- (42) Jameson, G. B.; Drago, R. S. *J. Am. Chem. Soc.* **1985**, *107*, 3017.
- (43) Koh, A. K.; Miller, D. J. *At. Data Nucl. Data Tables* **1985**, *33*, 235.
- (44) Hurst, G. C.; Henderson, T. A.; Kreilick, R. W. *J. Am. Chem. Soc.* **1985**, *107*, 7294.
- (45) Garcia, M. L. S.; Smith, J. A. S.; Bavin, P. M. G.; Ganellin, C. R. *J. Chem. Soc., Perkin Trans. 2*, **1983**, 1391.
- (46) Hsieh, Y.-N.; Rubenacker, G. V.; Cheng, C. P.; Brown, T. L. *J. Am. Chem. Soc.* **1977**, *99*, 1384.
- (47) Rudin, M.; Schweiger, A.; Günthard, Hs. H. *Mol. Phys.* **1982**, *46*, 1027.
- (48) Rudin, M.; Schweiger, A.; Günthard, Hs. H. *Mol. Phys.* **1982**, *47*, 171.